Journal of Magnetic Resonance **142,** 331–340 (2000)
doi:10.1006/jmre.1999.1944, available online at http://www.idealibrary.com on IDEAL®

Dead-Time Free Measurement of Dipole–Dipole Interactions between Electron Spins

M. Pannier, S. Veit, A. Godt, G. Jeschke, and H. W. Spiess

Max-Planck-Institut für Polymerforschung, Postfach 3148, 55021 Mainz, Germany

Received July 2, 1999; revised September 17, 1999

A four-pulse version of the pulse double electron–electron resonance (DEER) experiment is presented, which is designed for the determination of interradical distances on a nanoscopic length-scale. With the new pulse sequence electron–electron couplings can be studied without dead-time artifacts, so that even broad distributions of electron–electron distances can be characterized. A version of the experiment that uses a pulse train in the detection period exhibits improved signal-to-noise ratio. Tests on two nitroxide biradicals with known length indicate that the accessible range of distances extends from about 1.5 to 8 nm. The four-pulse DEER spectra of an ionic spin probe in an ionomer exhibit features due to probe molecules situated both on the same and on different ion clusters. The former feature provides information on the cluster size and is inaccessible with previous methods. © 2000 Academic Press

Key Words: EPR spectroscopy; DEER; biradical; electron spin echo; distance measurement.

INTRODUCTION

The determination of distances in disordered solids is of fundamental interest. Structure–function relationships of biological systems can often be understood only if the distances between functional groups are known (*1*). Similarly, one needs information on the size and shape of nanoscopic structure elements in polymers, such as, for instance, ionic multiplets in ionomers, to understand their properties (*2, 3*). For such materials the application of classical scattering techniques is limited due to the lack of periodic structures. However, magnetic resonance methods for measuring distances require only local order, as they are based on short-range magnetic dipole–dipole interactions. Since the advent of the spin echo double resonance (*4, 5*) experiment, such methods have gained considerable importance in nuclear magnetic resonance (NMR) studies of powder samples and disordered solids (*6*).

A new field in distance determination has been opened recently by introducing multiple-quantum experiments that can determine proton–proton and carbon–proton distances within functional groups as well as connectivities between them (*7, 8*). However, NMR methods are typically sensitive to distances smaller than 1 nm. By using EPR (electron paramagnetic resonance) methods, the accessible distance range can be easily extended to several nanometers (*9, 10*).

In amorphous solids, inhomogeneous broadening of the EPR spectra hides the smaller electron–electron interactions, so that long interradical distances can only be studied by separating this interaction. One approach is to measure the relaxation times T_1 and T_m, as the dipolar coupling accelerates longitudinal relaxation and decreases the phase memory times T_m. This method has, for instance, been used for determining distances in spin-labeled iron porphyrins (*11*). A more direct access to dipolar couplings is gained by double resonance methods as 2 + 1 (*12*), double electron–electron resonance (DEER) (*13*), and multiple-quantum EPR (*14, 15*). In particular, the three-pulse DEER experiment has been used to measure the electron spin–spin interaction (*16–19*) in a number of systems in order to determine interradical distances.

Unfortunately, the dead time inherent in three-pulse DEER experiments prevents one from reliably recording the signal of broad electron–electron coupling distributions. To overcome this problem we propose here a four-pulse version of the DEER experiment. To improve sensitivity, the detection period can be extended by additional $\pi/2$ pulses forming a pulse train (*20, 21*). The new sequence has been tested with two nitroxide biradicals of known length. The determined distances are in good agreement with previous work or model calculations, and the Pake-type spectra of the dipolar coupling patterns could be obtained. The advantage of the new sequence of being able to measure broad dipolar spectra is demonstrated for a polymer system, a modified poly(isoprene) (PI) with an ionic endgroup for each chain (ionomer) (*22, 23*). The chains form ionic clusters as the ammonium end groups aggregate, and an ionic spin probe can be attached to them. Both the cluster size and the cluster-to-cluster distance can be obtained with the four-pulse DEER experiment in this situation.

PULSE PATTERN

In the following discussion, a system consisting of two electron spins $S^A = \frac{1}{2}$ and $S^B = \frac{1}{2}$ with electron Zeeman and electron dipole–dipole interaction between them is considered. The spins which possess the resonant microwave (mw) fre-

1090-7807/00 $35.00

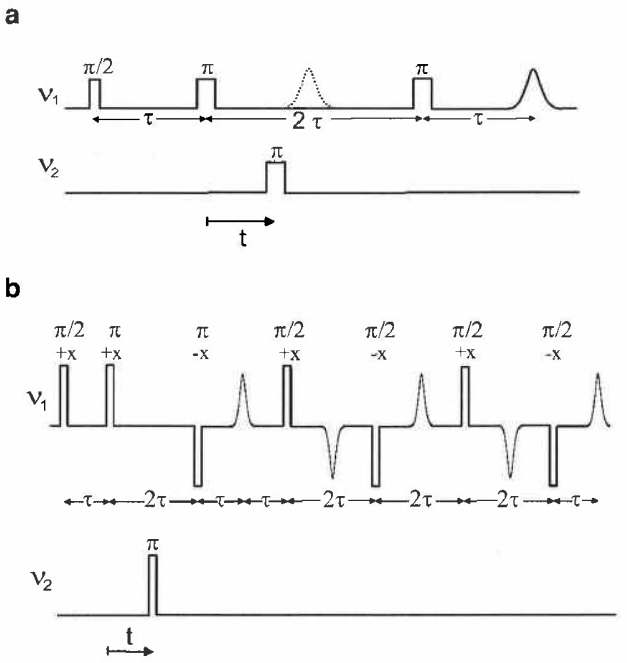

FIG. 1. Pulse patterns for dead-time-free DEER. (a) Four-pulse DEER. The time t between the second and third pulse of the sequence is incremented in steps of 8 ns. (b) Pulse-train DEER.

quency ν_{mw1} will be named A spins and the ones which possess the resonance frequency ν_{mw2} will be named B spins.

Four-Pulse DEER Experiment

The pulse pattern of the four-pulse DEER experiment is shown in Fig. 1a. At frequency ν_{mw1} a refocused Hahn-echo sequence is applied. In the vector picture of rotating frame, the first $\pi/2$ pulse (t_p = 32 ns) turns the magnetization of the A spins into the xy plane, so that the magnetization evolves under both the dipole–dipole interaction and the resonance offset $\Delta\omega_A$ of the A spins. After an evolution time of typically τ = 1000 ns the following π pulse (t_p = 32 ns) leads to an echo formation at time 2τ. The resulting electron spin echo (ESE) is shown in Fig. 1a (dotted echo). The final π pulse (t_p = 32 ns) at frequency ν_{mw1} is applied after an evolution time τ after the ESE and leads to a refocusing of the A spin magnetization at time τ after the last pulse.

The dipolar interaction can be studied if an additional π pulse (t_p = 32 ns) at the second irradiation frequency ν_{mw2} is inserted between the two π pulses at irradiation frequency ν_{mw1}; see Fig. 1a. This pulse is applied at the variable time t and affects only the B spins. The inversion of these B spins leads to a change of the local magnetic field at the A spins. As a result, the refocused ESE is a coherence transfer echo, which oscillates with the dipolar coupling frequency due to the variable time of flipping the B spins. In contrast to the three-pulse DEER experiment which lacks the first π pulse in ν_{mw1}, the maximum of the time domain signal can now be observed; it appears at time $t = \tau$ referred to the position of the π pulse (t_p = 32 ns) at frequency ν_{mw2}. The advantage of this new sequence is that it is a constant time experiment, where additional relaxation effects can be excluded and the complete electron-coherence pathway is symmetric, shown in Fig. 2, which is a well-known principle of designing pulse sequences in NMR; see, for example, the development of the NMR 2D-exchange pulse sequences for detecting motional processes (*24*). In contrast, the maximum time domain signal in the three-pulse experiment appears at t = 0. This time is experimentally not accessible because of the finite length of the mw pulse. Distortions of the signal occur as long as the pulse on the second frequency overlaps significantly with the falling edge of the pulse on the first frequency. This leads to dead times of about 64 ns for a loaded Q value $Q_L \approx 100$ of the resonator. Therefore the important first data points are lost in the three-pulse experiment.

Comparison with the HYSCORE Experiment

Due to pulse imperfections and a partial overlap of the excitation bands of pulses at ν_{mw1} and ν_{mw2}, the DEER sequence can also act as a HYSCORE experiment (*25–27*). HYSCORE measures nuclear frequencies which are about 14.8 MHz for weakly coupled protons at a static field of B_0 = 345 mT. The main difference between the two experiments is that the HYSCORE experiment measures the modulation of the *stimulated echo,* while the four-pulse DEER experiment observes the modulation of the *refocused echo.* Since the refocused echo and the stimulated echo appear at the same time using the new pulse sequence described here, the HYSCORE signal is observed in our measurements, too. This additional modulation can significantly distort the desired four-pulse DEER signal. Fortunately, there is a way for suppressing the HYSCORE signal. The HYSCORE formula (*26, 27*) shows that there are blind spots which can be induced by a suitable choice of the evolution time between the first and the second $\pi/2$ pulses. This approach proved to be more efficient than using phase cycling to separate the stimulated and refocused echo. This is possibly because there are also other pathways that lead to nuclear modulations and cannot be suppressed by phase cycling but exhibit similar blind spot behavior. For instance, nuclear modulations have also been observed with the 2 + 1 sequence (*28*). If it is possible to excite the dipolar spectrum

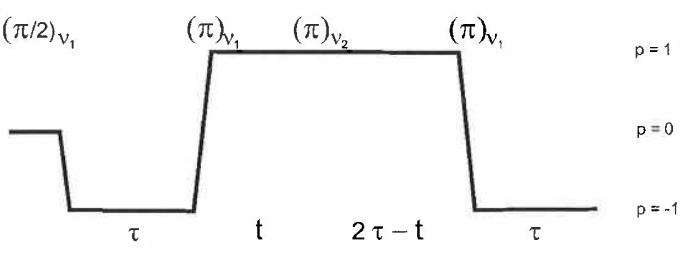

FIG. 2. Coherence pathway of the four-pulse DEER experiment.

with long mw pulses ($t_p \geq 40$ ns), the proton modulation can be completely avoided, as the modulation occurs only for mw pulses with sufficient excitation bandwidth (*29*).

Dipolar Modulated Echo Train

The signal-to-noise ratio can be improved by applying a new pulse train sequence for detection; see Fig. 1b. Each of the multiple echoes exhibits the desired dipolar modulation. The coherence pathway for the pulse train is the same as for the four-pulse DEER experiment just until the third mw pulse at frequency ν_{mw1} is irradiated. This pulse also acts like a $\pi/2$ pulse and stores magnetization in longitudinal direction, since off-resonance effects lead to a flip angle distribution. The longitudinal magnetization is now amplitude modulated with the dipolar coupling frequency with respect to the position of the π pulse at frequency ν_{mw2}. The next $\pi/2$ pulse (fourth pulse at frequency ν_{mw1}) transfers this magnetization back to transverse magnetization, which results in the formation of a stimulated echo. Each following $\pi/2$ pulse is acting in the same manner; it changes longitudinal magnetization into transverse one and generates an echo. At the same time, it stores back transverse magnetization to longitudinal one, which can again be recalled by the later $\pi/2$ pulses. This was checked by interpulse delays for which the refocused echo and the stimulated echo were separated. Accordingly, the echo train decays with a time constant closer to the longitudinal relaxation time T_1 than to T_m. As every echo is modulated with the dipolar coupling frequency, the gain in signal-to-noise ratio is given by

$$\frac{(S/N)_{PT}}{(S/N)_0} = \left(\frac{\sum_{i=1}^{n} I_n}{I_1}\right)^{1/2}, \qquad [1]$$

where I_1 is the intensity of the first echo and I_n is the intensity of the nth echo.

MODEL SYSTEM

The theory of the conventional three-pulse DEER experiment has already been described in some detail by Milov *et al.* and Larsen *et al.* (*13, 16*). We use the formalism of Pfannebecker *et al.* (*18*) for understanding the new pulse sequence. For simplicity, we restrict our consideration to an isolated electron–electron two-spin system $S^A = \frac{1}{2}$ and $S^B = \frac{1}{2}$. The considered interactions are electron Zeeman interaction and dipole–dipole interaction between the two electrons. The Hamiltonian in the high-field approximation in angular frequencies for this system is

$$\mathcal{H} = \omega_A S_z^A + \omega_B S_z^B + \omega_{AB} S_z^A S_z^B, \qquad [2]$$

where ω_A and ω_B describe the resonance frequency of the spin species A and B and ω_{AB} the dipolar coupling between them, given by

$$\omega_{AB} = \omega_{dip}(3\cos^2\theta_{AB} - 1), \qquad [3]$$

where the dipolar coupling frequency ω_{dip} is

$$\omega_{dip} = \frac{\mu_B^2 g_A g_B}{\hbar}\frac{1}{r_{AB}^3}, \qquad [4]$$

where μ_B is the Bohr magneton, g_A and g_B are the g factors of the respective electron, r_{AB} is the electron–electron distance, and θ_{AB} is the angle between the dipolar axis which connects the loci of both electrons and the magnetic field $\mathbf{B}_0$. The experiment can be explained by using the rotating frame picture, in which the Hamiltonian for spin A is written as

$$H'_{DEER} = \Delta\omega_A S_z^A + \omega_{AB} S_z^A S_z^B, \qquad [5]$$

where $\Delta\omega_A$ is the resonance offset, $\Delta\omega_A = \omega_A - \omega_{mw}$, and ω_{mw} is the mw carrier frequency. Only the terms which affect the A spins need to be considered, since any coherence of B spins generated during the pulse sequence does not contribute to the signal. The dipolar interaction leads to a splitting of each transition with the A spin frequencies $\omega_A^{\pm} = \Delta\omega_A \pm \frac{1}{2}\omega_{AB}$. The first $\pi/2$ pulse generates electron coherences evolving with ω_A^+ and ω_A^-, respectively. The following π pulse leads to an inversion of the evolving electron coherence, but the decisive pulse is the π pulse at mw frequency ω_{mw2} at the variable time t. An *electron coherence transfer* is induced by this π pulse and the electron coherence formerly evolving with ω_A^+ and ω_A^- evolves after this pulse with ω_A^- or ω_A^+, respectively. The final π pulse at frequency ω_{mw1} induces again an inversion of the phase of the electron coherence which leads to an electron spin echo. This refocused echo appears at time 4τ (see Fig. 1a) and its phase is given by

$$\begin{aligned}\varphi(4\tau) &= \omega_A^{\pm}\tau - \omega_A^{\pm}t - \omega_A^{\mp}(2\tau - t) + \omega_A^{\mp}\tau \\ &= \pm\omega_{AB}(\tau - t). \end{aligned} \qquad [6]$$

For the echo intensity, normalized to the intensity at $t = \tau$, we find

$$I(t) = \cos(\omega_{AB}(\tau - t)), \qquad [7]$$

i.e., a modulation with the dipolar coupling.

In a powder sample the dipolar coupling frequency ω_{AB} varies according to the orientation of the dipolar axis, so that the expected dipolar spectrum is the Pake spectrum. Observation of the complete Pake pattern would require that spins at all angles between the dipolar axis $\mathbf{r}$ and the magnetic field $\mathbf{B}_0$ can be excited, which may often not be the case (see below). The four-pulse DEER spectrum obtained by Fourier transform of the time domain signal, however, always exhibits the singu-

larities of the Pake pattern, from which the electron–electron distance can be determined.

Not only the coupling of the intramolecular neighbors within the same biradical contributes to the DEER signal. In addition, the coupling between the observed electron spin and every other electron spin in the sample must be taken into account. The electron–electron distances for this intermolecular contribution are usually statistically distributed, and this leads to a damping of the signal. For a homogeneous distribution of radicals, this part can be written as

$$I_{\text{intermol}}(t) = \exp(-kCF_B|\tau - t|), \qquad [8]$$

with

$$k = \frac{8\pi^2\mu_{\text{Bohr}}^2 g_A g_B}{9\sqrt{3}\,\hbar}, \qquad [9]$$

where C denotes the concentration of the unpaired electron spins and F_B is the fraction of electron spins excited by the mw pulse at frequency ν_{mw2} (*30*). This contribution to the decay is called instantaneous diffusion and can at least partially be suppressed at the expense of the signal-to-noise ratio by diluting the sample. The four-pulse DEER time domain signal is then given by

$$I_{\text{DEER}} = I_{\text{intramol}} I_{\text{intermol}}$$
$$= \cos(\omega_{AB}(\tau - t))\exp(-kCF_B|\tau - t|), \qquad [10]$$

so that in the spectrum the peak at ω_{AB} is convoluted with a Lorentzian line of width about 0.3 MHz (FWHM) for typical experimental conditions. In biradical samples there is also an unmodulated part due to those radicals where the second nitroxide moiety is outside the excitation range of the pulses at ν_{mw2}. This would lead to a strong peak at zero frequency. This peak can be removed by fitting and subtracting the exponential (see Experimental).

EXCITATION PROFILES

The rectangular mw $\pi/2$ and π pulses of duration t_p and $2t_p$, respectively, excite only a part of the EPR spectra. For each pulse sequence the excitation profile can be calculated (*31, 32*). For the A spins, the excitation function of the refocused echo pulse sequence is

$$f_A(\Delta\omega_A) = \left(\frac{\omega_1}{\omega_{\text{eff}}}\right)^5 \sin^5(\omega_{\text{eff}}t_p)\, g(\Delta\omega_A), \qquad [11]$$

with $\omega_{\text{eff}} = (\Delta\omega_A^2 + \omega_1^2)^{1/2}$, where ω_1 is the field strength of the mw pulse, ω_A is the resonance frequency of the A spins, ω_{eff} is the effective nutation frequency, and $g(\Delta\omega_A)$ is the EPR lineshape function. For the B spins, the excitation function according to the single π pulse of duration $2t_p$ is (*33*)

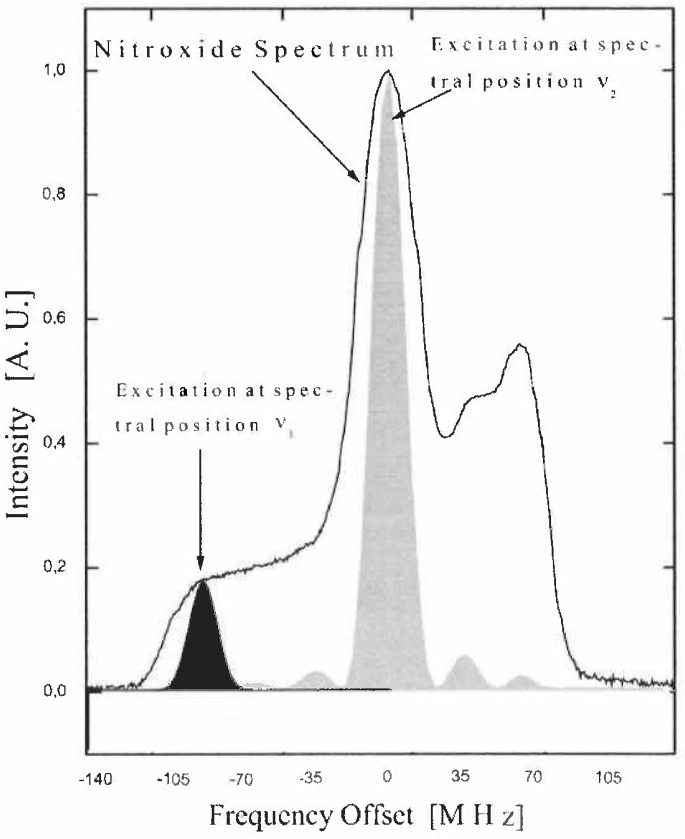

FIG. 3. Excitation profiles of the mw pulses within the ^{14}N-nitroxide spectrum.

$$f_B(\Delta\omega_B) = \left(\frac{\omega_1}{\omega_{\text{eff}}}\right)^2 \sin^2(\omega_{\text{eff}}t_p)\, g(\Delta\omega_B), \qquad [12]$$

with $\omega_{\text{eff}} = (\Delta\omega_B^2 + \omega_1^2)^{1/2}$ and $\Delta\omega_B$ is the resonance offset of the B spins. These excitation profiles are shown in Fig. 3. The difference of the two mw frequencies ω_A and ω_B should be sufficiently large so that the excitation profiles have almost no spectral overlap. Otherwise unwanted magnetization pathways can lead to artifact signals.

The knowledge of these excitation functions and their spectral position together with the resonator bandwidth allows one to calculate the range of angles θ_{CNC} through which radical fragments are excited. The angle θ_{CNC} is here the angle between a perpendicular of the C–N–C plane of the radical fragment and the magnetic field $\mathbf{B}_0$.

NUMERICAL AND ANALYTICAL CALCULATIONS

Numerical Simulation

Simulations of DEER traces were done by dividing the whole sequence into parts with time-independent Hamiltoni-

ans, so that the evolution of the density matrix for each part could be expressed by

$$\sigma(t) = \exp\left\{\frac{-i\mathcal{H}t}{\hbar}\right\}\sigma(t=0)\exp\left\{\frac{i\mathcal{H}t}{\hbar}\right\}. \quad [13]$$

For calculating the evolution of the density matrix of the spin system, the software package GAMMA (*34*) was used. An anisotropic dipole–dipole interaction was assumed for a two-spin system $S^A = \frac{1}{2}$ and $S^B = \frac{1}{2}$ with the Hamiltonian shown in Eq. [2]. The evolution during the mw pulses was described by the Hamiltonian

$$H_{\text{pulse}}^{\beta,\nu_\alpha} = \omega_1 S_i^j + H'_{\text{DEER}}, \quad [14]$$

where ω_1 is the field strength of the mw pulse, ν_α indicates at which mw frequency the pulse is irradiated, i indicates the affected spin (A or B), and j indicates the axis around which the spin is turned (x, y, or z). The density matrix was calculated for each position of the π pulse at frequency ν_{mw2}, the resulting signal for, e.g., magnetization in x direction was obtained according to $\langle S_x^A \rangle = \text{trace}\{\sigma S_x^A\}$.

In addition, the simulation considers orientation selection in the powder averaging due to the excitation profiles. The mw pulse selects certain values of the angle θ_{CNC}. Usually, θ_{CNC} is different for each of the two radical fragments due to the conformation of the molecule. For rigid biradicals, the orientations of the two radical sites are correlated with the inter-radical vector that includes the angle θ_{AB} with the magnetic field axis. The selective mw pulses irradiate only near-resonant spin species, which leads to a selection of nitroxide radical orientations. Which distribution of angles θ_{CNC} is selected by the excitation profiles is determined by the spectral position of the excitation profile within the EPR spectrum. For a biradical conformation where the C–N–C planes of both radical fragments lie in the same plane, the effect of the θ_{CNC} selection for each radical fragment leads to a distorted Pake spectrum, so that high coupling frequencies ($\sim 2\omega_{\text{dip}}$) are not observable. On the other hand, radicals with angle $\theta = 90°$ are almost always excited, so the typical singularity of the Pake spectra always appears and the electron–electron distance can be determined. The dipolar spectrum is obtained by Fourier transformation.

The results show that the four-pulse DEER experiment more faithfully than the three-pulse DEER experiment reproduces the orientation-selected Pake spectrum because of avoiding dead-time artifacts. This also indicates that the new four-pulse DEER can characterize distributions of the dipolar interaction.

Analytical Calculation

Calculations of DEER traces were done by using the product operator formalism and calculating directly the appearing commutators. For this the pulse sequence was divided into parts as discussed above. An extension for the software package Mathematica, SOME (*35*), was used that implements product operator formalism. The analytical result for a two-spin system after applying the four-pulse DEER sequence is

$$I_{4p\text{DEER}} = \cos(\omega_{\text{AB}}(2t - 3\tau + t_1)/2), \quad [15]$$

where t is the time as indicated in Fig. 1 and t_1 is the time after the last π pulse of the sequence. Therefore, the observed echo and not only its envelope is modulated with the dipolar coupling frequency ω_{AB}. Care must be taken in recording the signal, as the width and position of the integration boxcar influence the observable coupling frequencies (*36*), as earlier found for nuclear modulations. For the case of $t_1 = \tau$, the former equation reduces to Eq. [7].

EXPERIMENTAL

EPR Measurements

The four-pulse DEER measurements were performed on a modified Bruker ESP380E X-Band Fourier transformation spectrometer. The second frequency was fed into one channel of the microwave pulse forming unit. An HP-86290B RF plug-in module in an HP8350B sweep oscillator (2.0–18.6 GHz) was employed as the source for the second frequency. The output mw of the HP86290B plug-in module was increased by an amplifier from Miteq (AMF-5S-8012-18). A commercial electron nuclear double resonance resonator from Bruker (EN4118X-MD4) was used as a probehead, which was overcoupled for obtaining a broad resonator resonance line. The correspondingly lower Q_L value (about 100) leads to a loss of signal. However, handling a single-mode mw resonator proved to be more convenient and reliable compared to a bimodal resonator used before (*18*). In contrast to previous works, the position of irradiating the A spins is now located in the left shoulder of the nitroxide spectrum; see Fig. 2. Accordingly, the number of flipped B spins is increased and therefore the modulation depth and the signal-to-noise ratio are increased. The resolution of the four-pulse DEER experiment depends on the length of the constant time interval 2 τ, which in turn necessitated a measurement temperature of T = 15 K to ensure that enough signal was left despite phase relaxation for a period of 4 τ. The choice of a difference of 60 MHz between the two microwave frequencies enabled us to work with a single-mode resonator yet still excite transitions of the two nitroxide moieties selectively.

Sample Preparation

Two biradicals have been studied, the biradical 2,6-bis[(((2,2,5,5-tetramethyl-1-oxypyrrolin-3-yl) carbonyl) oxy)-antrachinon (see Fig. 4, compound **1,** synthesis described in (*16*)), and an additional nitroxide biradical; see Fig. 4, compound **3b.** A rigid biradical **2** studied earlier (*19*) is also included.

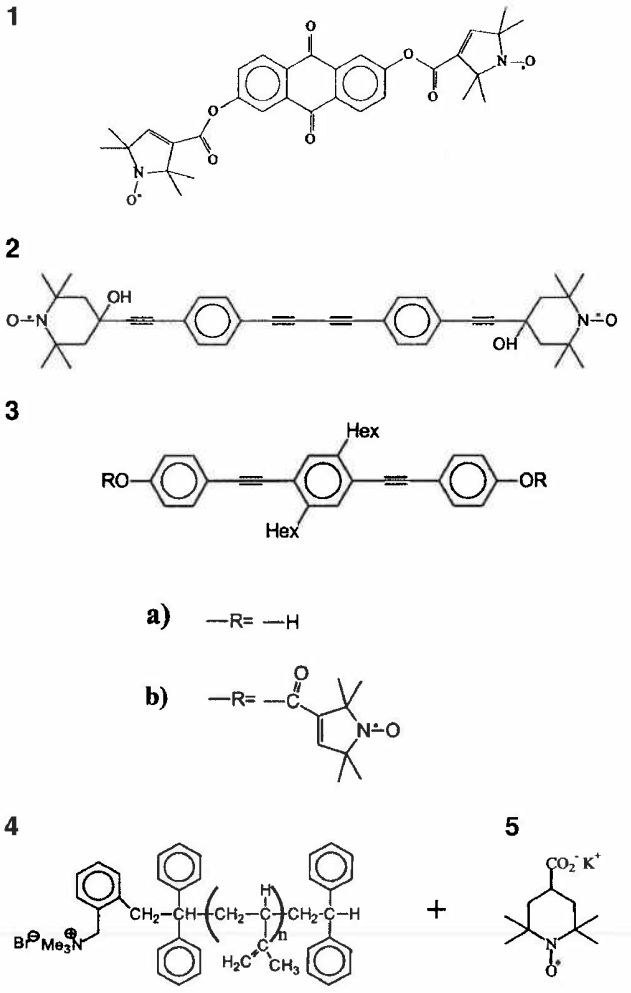

FIG. 4. Investigated systems. **1, 2,** and **3b** are rigid biradicals; **4** is an ionomer (left) to which the spin probe **5** (right) was added.

The monoradical TEMPO was used for comparison. All radicals were mixed into poly(styrene) with a molar fraction of 10^{-3} referred to the molecular weight of the poly(styrene) monomer (104 g/mol). Diluting radicals into a suitable polymer serves to increase the lifetime of the radicals, as motional processes are hindered and no oxygen can penetrate the sample.

For demonstrating the accessibility of broad distance distributions, an ionomer system was used. A poly(isoprene) chain was labeled with an ionic ammonium endgroup (see Fig. 4, compound **4**). In the polymer, the end groups aggregate and form ionic clusters (*37*). 4-Carboxy-TEMPO was neutralized with KOH to give its potassium salt (see Fig. 4, compound **5**), and **5** was then added to the polymer **4.** This probe molecule is built into the ionic cluster instead of one chain end, as has been proved by the temperature dependence of cw EPR spectra (*23*). If on average about two radicals are attached to the same ionic cluster, the size of the cluster can be determined and, in addition, the cluster-to-cluster distance can be obtained. Both distances exhibit a broad distribution.

Synthesis of Biradical 3b

To a cooled (ice bath) solution of 3-carboxy-2,2,5,5-tetramethylpyrroline-1-oxyl (*38*) (219 mg, 1.19 mmol) in dry THF (10 mL) were added subsequently dry pyridine (0.2 mL 2.5 mmol) and oxalyl chloride (0.1 mL, 1.16 mmol). After 1.5 h at room temperature, the turbid reaction mixture was cooled again with an ice bath and **3a** (130 mg, 0.27 mmol) followed by 4-*N,N*-dimethylaminopyridine (30 mg, 0.22 mmol) was added. The reaction mixture was stirred at room temperature for 28 h. It was quenched with 2 N HCl at 273 K and the product was extracted into diethyl ether. The combined organic phases were washed with saturated aqueous NaCl and dried ($MgSO_4$). Chromatography [neutral aluminium oxide S (Riedel de Haen), diethyl ether] gave biradical **3b** (111 mg, 50%) as a yellow solid. Crystals for X-ray analysis were obtained by recrystallization in ethanol containing a small amount of ethyl acetate. The structure as obtained by X-ray crystallography is shown in Fig. 5. NMR spectra were recorded on a Bruker AMX-300 MHz at room temperature in CD_2Cl_2. ^{1}H NMR: δ = 0.92 (6 H), 1.38 (15 H), 1.74 (4 H), 2.86 (4 H), 7.21 (very broad, 4 H), 7.42 (2 H), 7.63 (4 H); all signals are broad and structureless. ^{13}C NMR: δ = 13.2 (CH_3, 22.0, 28.5, 30.0, 31.1, and 33.4 (5 CH_2), 87.9 (C), 92.3 (C), 120.7, 121.6, and 121.8 (3 CH), 131.7 (CH), 132.0 (CH), 141.8 (C), 148.4 (broad; C). The substitution degree of carbon (C, CH, CH_2, CH_3) was determined by a DEPT experiment. $C_{52}H_{62}O_6N_2$ (811.1): FD-MS: m/z = 810.5 (100%).

RESULTS AND DISCUSSION

Model Compound

Biradical **1** was used as a model compound because of its known end-to-end distance (*16, 18*). This sample was also used for determining the optimum experimental conditions. Its four-pulse DEER signal at 15 K is shown in Fig. 6a. The amplitude modulation corresponds to the intramolecular electron–electron coupling and reflects the electron–electron distance, while the exponential decay corresponds to the intermolecular coupling of electrons located at different molecules. The intermolecular part was eliminated by fitting the exponential decay and subtracting it. This method has been shown to work more reliably than division by the exponential (deconvolution) in the field of electron spin echo envelope modulation spectroscopy (*39*). The resulting modulation is shown in Fig. 6b.

The size of the time domain data set was doubled by zero filling and then the cosine spectrum was obtained by Fourier transformation. The dipolar spectrum of compound **1,** see Fig. 7a, is similar to the theoretically expected Pake spectrum. The singularities which define the dipolar coupling constant and thus the electron–electron distance are very well recognizable. Only the "foot" of the Pake spectrum is not visible. This is due to orientation selection in agreement with theoretical considerations above. The spectral position and the width of the singularity is a hint to

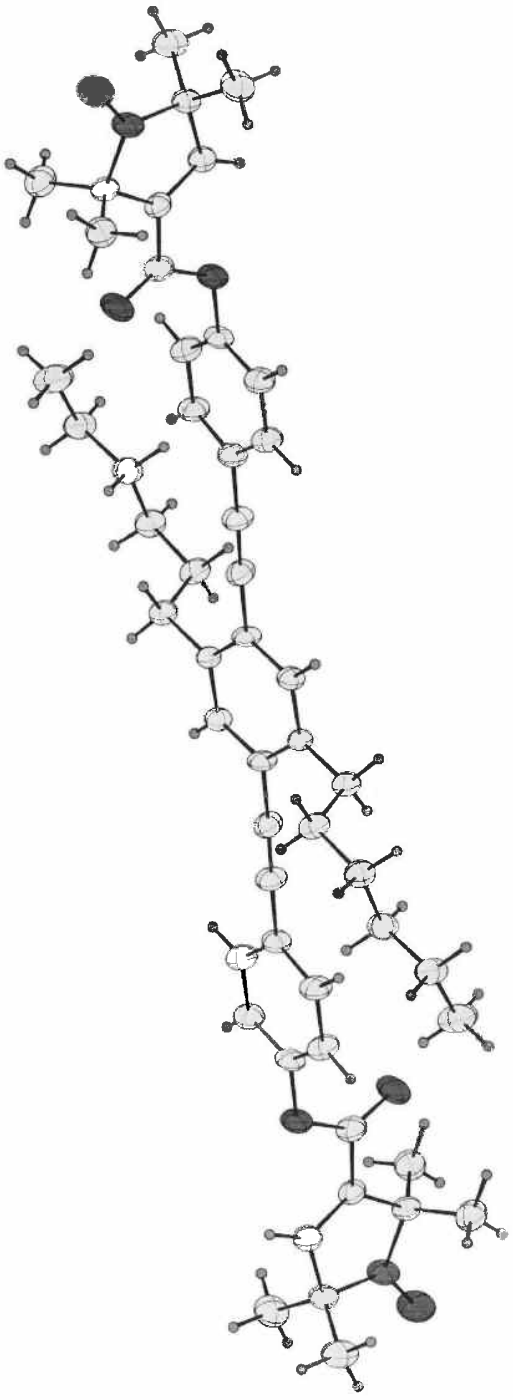

FIG. 5. Structure of biradical **3b** as determined by single-crystal X-ray diffraction.

the conformation of the studied molecule. For several distinct conformations, more than one singularity is expected in the spectrum. If there is a distribution of conformations, a broadening of the singularity appears due to the addition of all possible Pake spectra. Therefore, the width of the singularity corresponds to the electron–electron distance distribution, at least in the limit of low concentration where it is not dominated by the convolution with the unspecific decay due to statistically distributed electron spins. In our case, the small width indicates that the biradical **1** possesses only one conformation.

A very well-defined Pake spectrum has also been observed with four-pulse DEER on a rigid-rod biradical **3b** with nitroxide endgroups; see Fig. 6b. The result of $r_{12} = 1.94$ nm for the biradical **1** is in very good agreement with previous measurements, while the result for **3b,** $r = 2.83$ nm, is in agreement with X-ray diffraction results; see Table 1.

Application to Distance Distributions: Ionomers

The time domain signal for the functionalized poly(isoprene) sample **4** is shown in Fig. 8. The shaded area in the center of

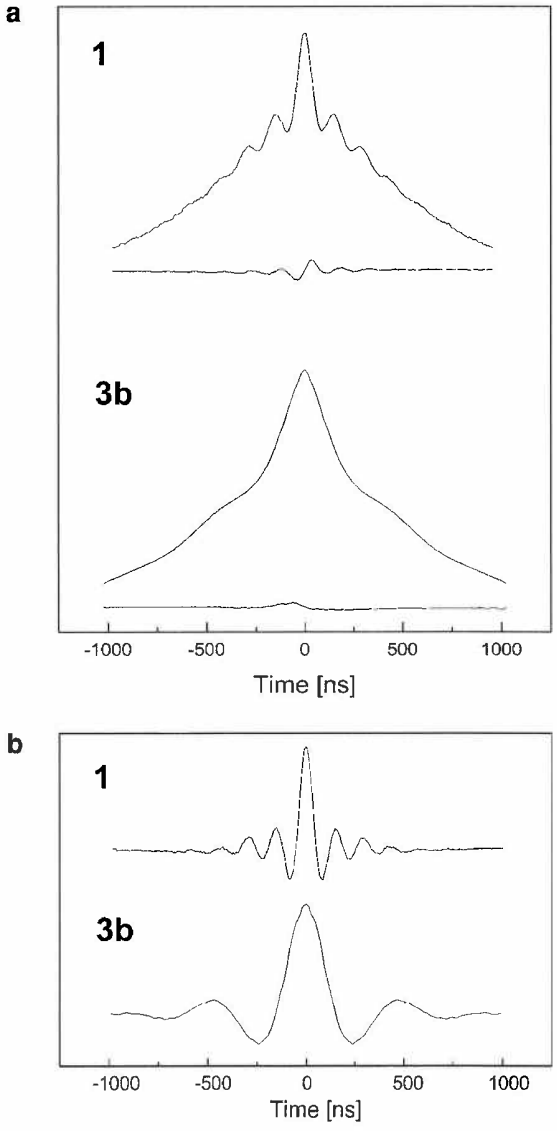

FIG. 6. Four-pulse DEER time domain signals of the biradicals under investigation. (a) Raw data, the upper trace is the real part, the lower one the imaginary part of the time domain signal for biradicals **1** and **3b.** (b) Pure dipolar modulations after fitting and subtracting the exponential corresponding to intermolecular interactions.

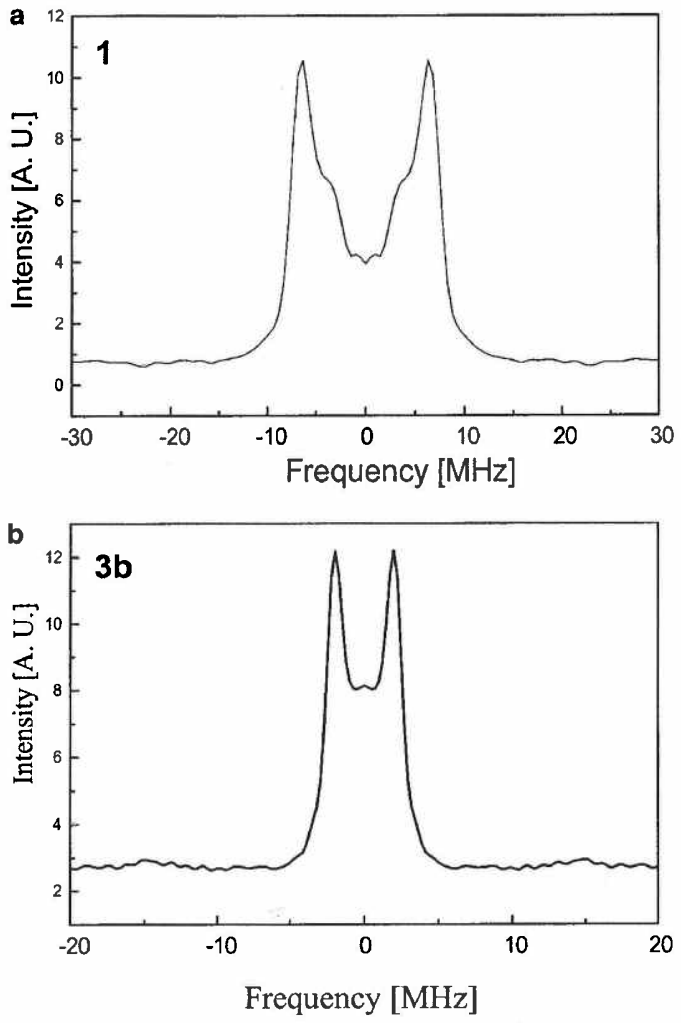

FIG. 7. Spectra obtained by Fourier transformation of the modulation patterns shown in Fig. 6b, (a) compound **1,** (b) compound **3b.** Deviations from the ideal Pake spectrum are due to orientation selection. The position of the singularity defines the electron–electron distance.

the signal indicates the dead time of the three-pulse DEER experiment and demonstrates clearly that the most prominent characteristic feature would be almost completely hidden. This peak in the center contains information about the cluster size, whereas the longer lasting bow contains information about the cluster-to-cluster distance. For obtaining these distances, the time domain signal has been fitted by a simulation program, which will be described in more detail elsewhere. The measured radical–radical distances within the cluster is 2.2 nm, and the cluster-to-cluster distance for system **4** is (6.6 ± 0.5) nm, which is in good agreement with results obtained by small angle X-ray scattering (SAXS) for similar systems.

In accessing small distances, a bandwidth problem occurs as the lower limit for the π pulse lengths is $t_p = 32$ ns with our spectrometer, and therefore dipolar subspectra wider than approximately 25 MHz could not be excited. Therefore distances shorter than 1.5 nm can not be studied with our experimental setup. The upper distance limit is determined by the sensitivity of the new four-pulse sequence, which depends on the phase memory time (T_m). The whole duration 4τ should not considerably exceed T_m, so that the upper distance limit is expected to be at about 8 nm for nitroxide radicals with similar phase memory times T_m as observed in this work.

Signal Improvement through Echo Train

One way to improve the sensitivity is the application of the pulse-train sequence where the echos could still be observed until 60 μs after the first pulse. This is demonstrated in Fig. 9 for sample **1,** where the dipolar modulation on top of the first and the fifth echo is shown. As each echo is modulated with the dipolar coupling frequency, the gain in signal-to-noise ratio is a factor of about 2 if only the first 10 echos of the time domain signal shown in Fig. 9 are taken into account.

CONCLUSION

The new dead-time-free four-pulse DEER experiment was introduced and applied to two "rigid" biradicals of different length. Due to π bindings the biradicals are rigid. These results support and extend the findings in Ref. (*19*), where a whole series of rigid rod biradicals of different length has been studied. Electron–electron distances could be obtained from the Pake-type dipolar spectra. The results agree with previous DEER measurements or with model calculations of the molecules. For the first time the angular-dependent part of the DEER signal could be observed, and as a consequence Pake-type dipolar spectra could be presented. The signal-to-noise ratio was increased by irradiating the observer mw frequency at the flank of the EPR ^{14}N nitroxide spectrum and the pumping mw frequency at the center of the EPR spectrum in contrast to previous works. A further improvement was obtained by using a pulse train for detecting multiple modulated echoes.

The experimental data agree well with numerical simulations and analytical calculations of the four-pulse DEER se-

TABLE 1
Electron–Electron Distances of the Investigated Systems

Compound	ω_{DD} [MHz]	r_{12}^{th} [Å]	r_{12}^{exp} [Å]	Reference
1	7.12 ± 0.49	—	19.4 ± 0.5	This work
1	6.77 ± 0.14	—	19.73 ± 0.14[a]	(*16*)
2	3.05 ± 0.49	27.7 ± 1.0	25.7 ± 1.4	(*19*)
3b	2.29 ± 0.49	27.84 ± 0.01[b]	28.3 ± 0.5	This work
4[c]	4.9	—	22 ± 3	This work
4[d]	0.2	—	66 ± 5	This work

[a] Statistical error.
[b] X-ray diffraction, N–N distance.
[c] Rapid decay (cluster size).
[d] Slow modulation (cluster-to-cluster distance).

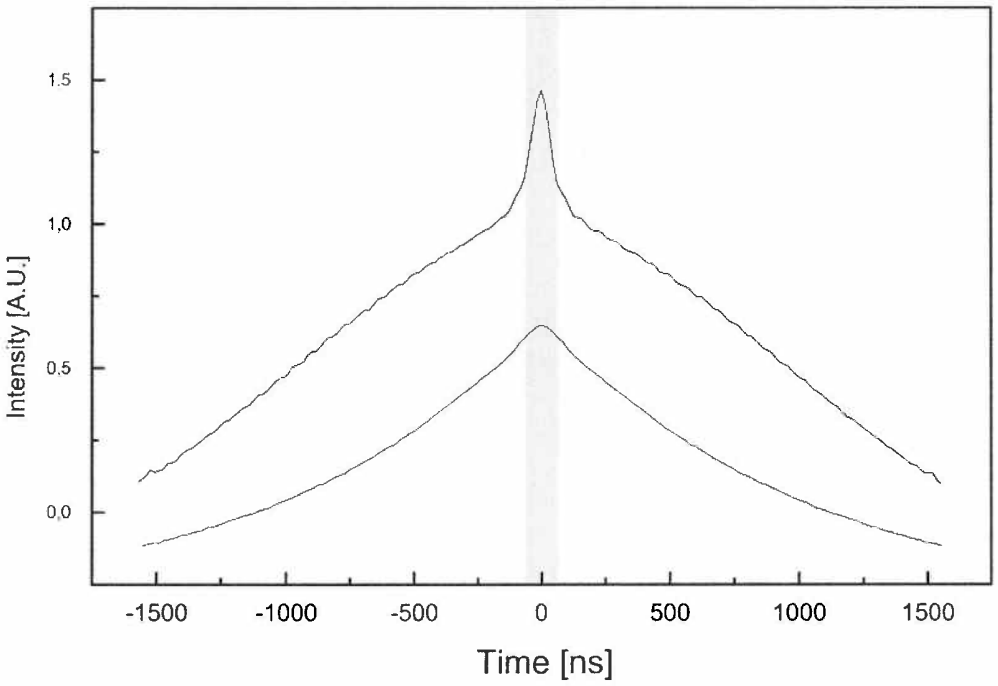

FIG. 8. Four-pulse DEER time domain signal of the ionomer **4,** upper trace. The lower trace is the time domain signal obtained for the statistically distributed monoradical TEMPO for comparison, only the exponential is visible. The shaded region corresponds to the dead time of the three-pulse DEER experiment. The narrow feature in the center is due to radicals attached to the same cluster, whereas the slow bow is due to radicals located at different clusters.

quence. Broad distance distributions are now accessible, as was demonstrated by determining the cluster size (about 2.2 nm) and cluster-to-cluster distances (about 6.6 nm) in an ionomer. The findings agree well with data obtained by SAXS measurements. The present study thus shows that intergroup distances of several nanometers can be determined and provides a basis for studying more complicated samples where electron–electron distances exhibit even broader distributions. Investigations on ionomers based on block copolymers are now in progress.

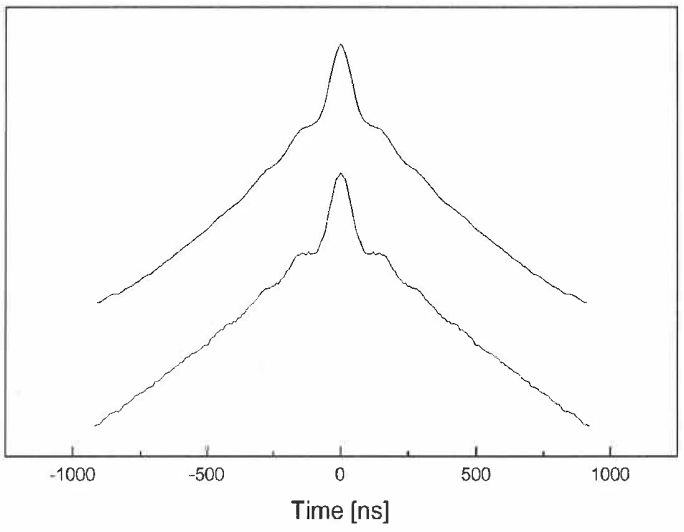

FIG. 9. Time domain signals of the pulse-train DEER sequence for biradical **1.** The first and the fifth echoes with their dipolar modulations are shown.

ACKNOWLEDGMENTS

The authors thank C. Bauer for modifying the mw bridge for irradiating the second mw frequency, R. Ulrich for synthesizing biradical **1,** R. Martin and F. Diederich for synthesizing biradical **2,** V. Schädler for synthesizing ionomer system **4,** V. Enkelmann for the X-ray crystallography, M. Hubrich for help in the early stages of the experiment, and U. Wiesner and A. Raitsimring for helpful discussions.

REFERENCES

1. Y.-K. Shin, C. Levinthal, F. Levinthal, and W. L. Hubbel, *Science* **259,** 960 (1993).
2. S. Schlick (Ed.), "Ionomers, Characterization, Theory, and Applications," CRC Press, New York (1996).
3. A. N. Semenov, L. A. Nrkova, and A. R. Khoklov, *Macromolecules* **28,** 7491 (1995).
4. D. E. Kaplan and E. L. Hahn, *J. Phys. Radium* **19,** 821 (1958).
5. M. Emshwiller and E. L. Hahn, *Phys. Rev.* **118,** 414 (1960).
6. T. Gullion and J. Schaefer, *in* "Advances in Magnetic Resonance" (W. S. Warren, Ed.), Vol. 13, p. 55, Academic Press, New York (1989).
7. J. Gottwald, D. E. Demco, R. Graf, and H. W. Spiess, *Chem. Phys. Lett.* **243,** 314 (1995).
8. R. Graf, D. E. Demco, J. Gottwald, S. Hafner, and H. W. Spiess, *J. Chem. Phys.* **106,** 885 (1997).
9. J. E. Wertz and J. R. Bolton, "Electron Spin Resonance," McGraw–Hill, New York (1972).

10. G. R. Eaton and S. S. Eaton, *in* "Biological Magnetic Resonance" (L. J. Berliner and J. Reuben, Eds.), Vol. 8, pp. 339–398, Plenum, New York (1989).
11. M. H. Rakowsky, K. M. More, A. V. Kulikov, G. R. Eaton, and S. S. Eaton, *J. Am. Chem. Soc.* **117,** 2049 (1995).
12. V. V. Kurshev, A. M. Raitsimring, and Y. D. Tsvetkov, *J. Magn. Reson.* **81,** 441 (1989).
13. (a) A. D. Milov, K. M. Salikhov, and M. D. Shirov, *Fiz. Tverd. Tela* **23,** 975 (1981); (b) A. D. Milov, A. B. Ponomarev, and Yu. D. Tsvetkov, *Chem. Phys. Lett.* **110,** 67 (1984).
14. S. Saxena and J. H. Freed, *Chem. Phys. Lett.* **251,** 102 (1996).
15. P. Borbat and J. H. Freed, *Chem. Phys. Lett.,* in press.
16. R. G. Larsen and D. J. Singel, *J. Chem. Phys.* **98,** 5134 (1993).
17. A. D. Milov, A. G. Maryasov, and Yu. D. Tsvetkov, *Appl. Magn. Reson.* **15,** 107 (1998).
18. V. Pfannebecker, H. Klos, M. Hubrich, T. Volkmer, A. Heuer, U. Wiesner, and H. W. Spiess, *J. Phys. Chem.* **100,** 13428 (1996).
19. R. E. Martin, M. Pannier, F. Diederich, V. Gramlich, M. Hubrich, and H. W. Spiess, *Angew. Chem. Int. Ed.* **37,** 2834 (1998).
20. H. Y. Carr and E. M. Purcell, *Phys. Rev.* **94,** 630 (1954).
21. S. Meiboom and D. Gill, *Rev. Sci. Instrum.* **29,** 688 (1958).
22. V. Schädler, A. Franck, U. Wiesner, and H. W. Spiess, *Macromolecules* **30,** 3832 (1997).
23. V. Schädler, V. Kniese, T. Thurn-Albrecht, U. Wiesner, and H. W. Spiess, *Macromolecules* **31,** 4828 (1998).
24. D. Schaefer, J. Leisen, and H. W. Spiess, *J. Magn. Reson. A* **115,** 60 (1994).
25. P. Höfer, A. Grupp, H. Nebenführ, and M. Mehring, *Chem. Phys. Lett.* **132,** 279 (1986).
26. C. Gemperle, G. Aebli, A. Schweiger, and R. R. Ernst, *J. Magn. Reson.* **88,** 241 (1990).
27. A. M. Tyryshkin, S. A. Dikanov, and D. Goldfarb, *J. Magn. Reson. A* **105,** 271 (1993).
28. A. M. Raitsimring, R. H. Crepeau, and J. H. Freed, *J. Chem. Phys.* **102,** 8746 (1995).
29. S. A. Dikanov and Yu. D. Tsvetkov, "Electron Spin Echo Envelope Modulation (ESEEM) Spectroscopy," Ch. 9, CRC Press, Boca Raton, FL (1992).
30. J. R. Klauder and P. W. Anderson, *Phys. Rev.* **125,** 912 (1962).
31. A. L. Bloom, *Phys. Rev.* **98,** 1105 (1955).
32. E. T. Jaynes, *Phys. Rev.* **98,** 1099 (1955).
33. A. Abragam, "The Principles of Nuclear Magnetism," Clarendon, Oxford (1983).
34. S. A. Smith, T. O. Levante, B. H. Meier, and R. R. Ernst, *J. Magn. Reson. A* **106,** 75 (1994).
35. S. Boentges, private communication.
36. C. Gemperle, A. Schweiger, and R. R. Ernst, *J. Magn. Reson.* **91,** 273 (1991).
37. J. S. Kim and A. Eisenberg, "Introduction to Ionomers," Wiley, New York (1998).
38. E. G. Rozantsev *in* "Free Nitroxyl Radicals" (B. J. Hazzards and H. Ulrich, Eds.), p. 206, Plenum, New York (1970).
39. R. P. J. Merks and R. de Beer, *J. Magn. Reson.* **37,** 305 (1980).